Charge ordering in θ-(BEDT-TTF)$_2$RbZn(SCN)$_4$ studied by vibrational spectroscopy

Kaoru Yamamoto* and Kyuya Yakushi
Institute for Molecular Science, Myodaiji, Okazaki, Aichi 444-8585, Japan

Kazuya Miyagawa and Kazushi Kanoda
Department of Applied Physics, The University of Tokyo, Bunkyo-ku, Tokyo 113-8656, Japan

Atsushi Kawamoto
Department of Physics, Hokkaido University, Kita-ku, Sapporo 060-0810, Japan

(Received 22 March 2001; revised manuscript received 8 August 2001; published 8 February 2002)

Charge distribution in the insulating phase of θ-(BEDT-TTF)$_2$RbZn(SCN)$_4$ [BEDT-TTF denotes bis(ethylenedithiolo)tetrathiafulvalene] is investigated using the polarized Raman and infrared (IR) spectroscopy. Both of the Raman and IR spectra showed a multiple-peaks pattern below metal-insulator transition temperature. We assigned the carbon-double-bond (C═C) stretching-modes based on the isotope shift in the ^{13}C-substituted sample, and performed a factor-group analysis for the polarized IR and Raman spectra. These results proved that charge disproportionation (CD) takes place in the insulating phase, and that the spatial pattern of the charge ordering agrees with the symmetry determined by the x-ray diffraction. The CD ratio was estimated from the frequency of a ring C═C stretching mode that is weakly coupled with electronic excited states. A systematic way to investigate the CD phenomenon based on vibrational spectroscopy is discussed.

DOI: 10.1103/PhysRevB.65.085110 PACS number(s): 71.30.+h, 71.27.+a, 71.38.−k

I. INTRODUCTION

Charge ordering draws a growing attention as a new electron-correlation phenomenon in organic charge-transfer (CT) salts.[1,2] θ-(BEDT-TTF)$_2$RbZn(SCN)$_4$ [BEDT-TTF denotes bis(ethylenedithiolo)tetrathiafulvalene, abbreviated to ET, hereafter] and its isostructural compounds have been studied as examples of two-dimensional (2D) charge-ordering system. The series of θ type of ET salts has been synthesized by Mori *et al.*[3,4] In these compounds, ET molecules are not dimerized but take a uniform herringbone arrangement. Since these compounds have a (3/4)-filled band with a closed Fermi surface according to the band calculation, they are expected to be stable metals. Actually, some of these salts show a metallic behavior. However, all compounds eventually become insulators at low temperatures. The charge gap responsible for the insulating behavior is ascribed to a certain charge localization, because these compounds remain paramagnetic in the insulating phase.[3] The most important difference from the Mott insulating state in κ-type ET salts[5] is in the characteristic charge distribution; charge disproportionation (CD) is suggested to occur in the insulating phase of the θ salts.

The charge localization found in the θ-type compounds has been investigated primarily by means of magnetic and theoretical methods. Nakamura *et al.* discovered a sign of CD in the angular dependence of the electron-spin-resonance spectrum of θ-(ET)$_2$CsZn(SCN)$_4$, which stimulated an interest in the CD phenomenon of the θ-type ET salts.[6] Miyagawa *et al.*[7] and Chiba *et al.*[8] performed the ^{13}C-nuclear-magnetic-resonance measurements for θ-(ET)$_2$RbZn(SCN)$_4$, and reported the existence of charge-rich and -poor sites in the insulating phase. Meanwhile, Seo and Fukuyama have carried out a mean-field calculation to understand the mechanism of the charge localization[9,10] and have proposed that a stripe-patterned charge ordering is stabilized in the insulating phase owing to intermolecular Coulomb repulsive forces. Recently, Mori *et al.* have proposed that the intermolecular Coulomb interaction can be estimated from the electrostatic energies between the point charges on a molecule calculated by the extended Hückel method.[11]

Among various approaches applicable to the research of the charge ordering,[12,13] vibrational spectroscopy can be one of the powerful methods[14] for the following reasons. First, the frequencies of the C═C stretching modes of ET sensitively shift depending on the charge population upon the molecule.[15–18] This property enables us to estimate the CD ratio. Second, the stretching mode of the central C═C bond of ET molecule strongly couples with charge-transfer excited states [electron-molecular vibration (EMV) coupling], generating a large factor-group splitting. As is widely known, the factor-group splitting tells us the unit-cell symmetry through the spectral selection rule. Because the selection rule is sensitive to the charge distribution, the vibrational spectra provide us essential information on the arrangement of equivalently charged molecules.

In the present paper, the polarized Raman and infrared (IR) spectra of θ-(ET)$_2$RbZn(SCN)$_4$ are studied to verify the presence of CD in the insulating phase and to determine the spatial pattern of the ordered charges from the vibrational analysis. Based on the results of the thorough investigation on the polarized spectra, we will discuss a systematic way to analyze the vibrational spectra of ET salts in charge ordering state. In Sec. III, we assign the Raman and IR spectra in the C═C stretching region with the aid of the isotope shift in the ^{13}C-substituted compound. Existence of the screw-axis symmetry is verified through the factor-group analysis in Sec. IV A. By using a cluster model, we confirm the occurrence of CD in Sec. IV B. Finally, the CD ratio is estimated

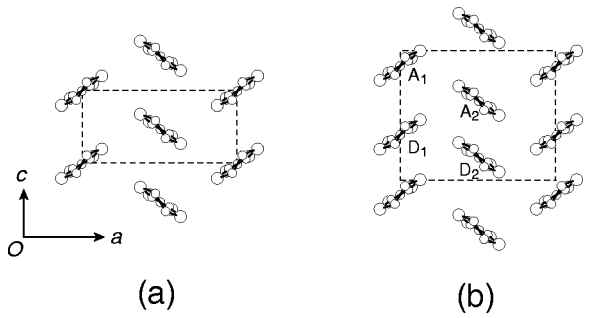

FIG. 1. Arrangement of ET molecules in the crystal of θ-$(ET)_2RbZn(SCN)_4$ (a) at room temperature and (b) below T_{MI}.

from the frequency of a certain C═C stretching mode in Sec. IV C.

II. EXPERIMENTAL

Single crystals of θ-$(ET)_2RbZn(SCN)_4$ were prepared following the reported procedure.[3] The average crystal size was ca. $1\times0.2\times0.02$ mm^3. The crystals were mounted by grease on an aluminum cold stage in a cryostat Oxford CF1104, and cooled down to 20 K. The temperature of the sample was measured with a silicon-diode sensor fixed to the cold stage. The cooling rate was controlled at ca. 2 K/h around the metal-to-insulator (MI) transition temperature T_{MI} in order to suppress the formation of a metastable state.[7,19] Raman spectra were collected using a Renishaw Ramascope System 1000 composed of a notch filter, single monochromator, and charge-coupled device cooled by a thermoelectric device. Excitation light from a He-Ne laser, NEC GLG5731 ($\lambda=632.8$ nm) was focused on a ca. 10-μm-diameter spot through a microscope equipped with an objective lens Mitsutoyo M Plan Apo 20x. The laser power was kept less than 75 μW to avoid overheating. The scattered light was collected with a backscattering geometry. In this paper, the polarizations of the incident and scattered light are referred to as, for example, (a,c) in the case that the incident and scattered light were polarized in the a and c axes, respectively. Each spectrum was collected with a 30 min accumulation. Infrared reflectance spectra were observed from 600 to 12000 cm^{-1} using a microscopic measurement system composed of an IR microscope Spectratech IR plan and a Four-transformed IR spectrometer Nicolet Magna 760. Samples were cooled with the same system used in the Raman measurement, except that a KBr crystalline plate coated with a waterproof film (TOPCON Co., Tokyo, Japan) was used as the optical window. Conductivity spectra were calculated through the Kramers-Kronig analysis from the reflectance spectra. Details of the reflectance measurements have been described elsewhere.[20]

III. RESULTS

A. Crystal structure and multiple C═C stretching peaks

Figure 1(a) shows the molecular arrangement of ETs in the crystal of θ-$(ET)_2RbZn(SCN)_4$ at room temperature.[4] The ET molecules are arranged in a herringbone pattern with their molecular long axis perpendicular to the plane of the donor layers. The (3/4)-filled band and the closed Fermi surface predicted by the tight-binding calculation[4] fulfill the conditions for a stable metal, but the crystal undergoes a first-order MI transition at around 150–190 K.[7,19] Lowering symmetry, the unit cell is doubled below T_{MI}. The doubled unit cell accommodates two pairs of crystallographically independent molecules A_n and D_n $(n=1,2)$ as shown in Fig. 1(b). Throughout this paper, we have employed the room-temperature notation of the crystal axes, though the space group is changed from $I222$ to $C2^4$ below T_{MI}.

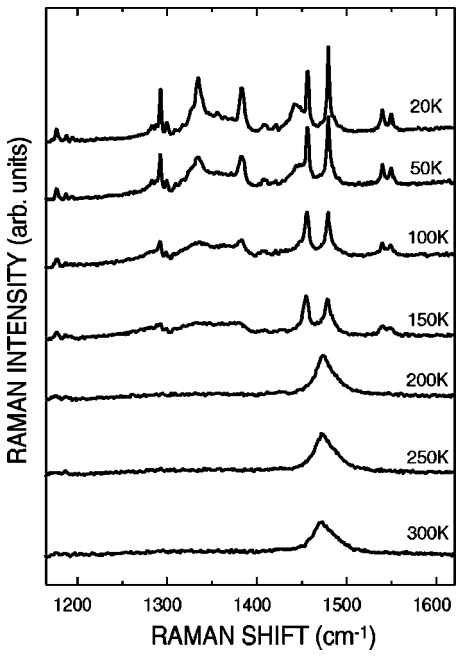

FIG. 2. Temperature dependence of the $(a,a+c)$-polarized Raman spectrum around the characteristic frequency for C═C stretching.

Figure 2 shows the temperature dependence of the Raman spectrum around the characteristic frequency of C═C stretchings. The spectrum observed above T_{MI} consists of a broadband centered at 1474 cm^{-1}. It changed to a multiple-peaks pattern below T_{MI}. Among the observed bands, the weak band at 1407 cm^{-1} and the bundle of sharp peaks at around 1290 cm^{-1} are attributed to the C-H bending modes $\nu_4(a_g)$ and $\nu_5(a_g)$, respectively, because the observed frequencies and the pattern agree with the reported features of these vibrational modes.[21] The multiple Raman signals cannot be explained in terms of the molecular symmetry. This is because an ET molecule has only three C═C stretching modes, even if we take into account one Raman inactive (ungerade) mode.

Figure 3 shows the optical conductivity spectra measured on the ac plane. The spectra exhibited a broad band at room temperature. The profile of the broad band is not simple Drude-like, but it indicates an energy continuum in the excited state. A very broad hump and dip were found around the C═C stretching region (ca. 1200 and 1500 cm^{-1}). These features may be ascribed to a vibronic effect caused by a structural fluctuation.[22] Though the spectra of the metallic

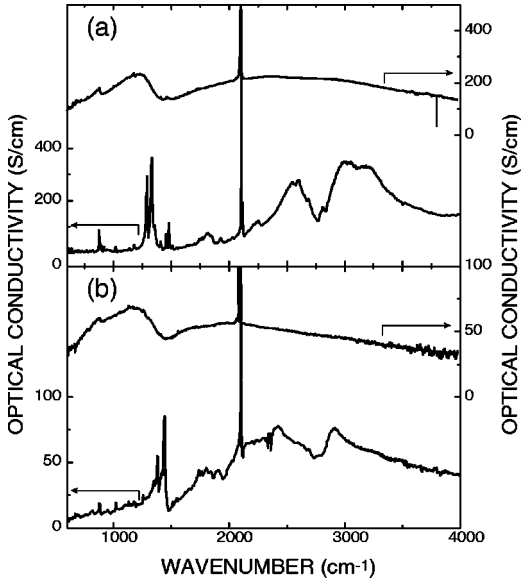

FIG. 3. Optical-conductivity spectra polarized parallel to (a) the *a* axis and (b) the *c* axis. Upper and lower curves in the two panels show the spectra measured at room temperature and 50 K, respectively.

phase are not well understood, we will devote our attention to the insulating phase in the present discussion. The conductivity spectra were significantly changed below T_{MI} [lower curves in Figs. 3(a) and 3(b)]; one can see the large high-frequency shift of the spectral weight and the emergence of the multiple-peaks similar to the Raman spectrum in the charge-gap region. Tajima *et al.* have argued the electronic excitation in the conductivity spectrum in terms of comparison with a theoretical calculation.[23] Here, we will focus our attention on the characteristic vibrational features to investigate the charge population on each ET molecule.

B. Isotope shift of the multiple C═C signals

According to the normal-mode analysis assuming the D_{2h} molecular symmetry,[24] the three C═C stretching modes of the ET molecule are classified into two gerade and one ungerade modes. Figure 4(a) shows the schematic atomic displacement in these modes. The two gerade modes, called ν_2 and ν_3, are composed of central and in-phase ring C═C stretchings, and the ungerade mode ν_{27} corresponds to antiphase ring C═C stretching. We performed the isotope-shift measurements using the ^{13}C-substituted sample to determine the assignment of the multiple peaks. As shown by the asterisks in Fig. 4(b), the two carbon atoms in the central C═C bond are replaced by ^{13}C atoms in the isotope-substituted sample. Because only the two gerade modes ν_2 and ν_3 include the central C═C bond stretching, these modes can be distinguished from the ungerade mode ν_{27} by the isotope-shift measurement. Moreover, it is possible from the isotope shift value to distinguish ν_3 from ν_2, since the contribution of the central C═C stretching in ν_3 is larger than that of ν_2.[21,25,26]

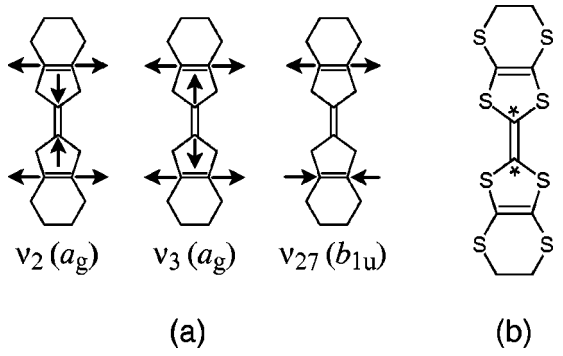

FIG. 4. (a) Schematic atomic displacement for the C═C stretching modes. (b) Molecular structure of the ^{13}C-substituted ET molecule (asterisks indicate ^{13}C atoms).

Figure 5 shows the polarized Raman and conductivity spectra of the natural (nonsubstituted) and ^{13}C-substituted samples. All peaks except for ν_4 and ν_5 showed isotope shift. Therefore, these peaks are attributed to the gerade modes ν_2 and ν_3. The ungerade ν_{27} mode, which is polarized along the molecular long axis, was found neither in the Raman nor in the IR spectra, because the molecular long axis is perpendicular to the *ac* crystal face. We labeled the C═C stretching peaks as shown in Fig. 5 to specify the peaks belonging to a common mode between the natural and substituted samples. The frequencies of these peaks are summarized in Table I together with the assignment. Correspondence of the peaks between the two samples was determined in the following manners. The lowest-frequency peaks of the two samples, $\mathbf{b}_2$ and $\mathbf{b}_2'$, are commonly found in the (a,a)- and (b^*,b^*)-polarized Raman spectra [See Figs. 5(a) and 5(c)] and *a*-polarized conductivity spectrum [Fig. 5(d)], where b^* denotes the direction perpendicular to the *ac* plane. The sharp ν_5 signals overlap these broad bands, making it difficult to determine the precise frequency difference between the two broad bands. However, it is certain that the difference is less than ca. 60 cm^{-1}, which is the maximum isotope shift expected for the local mode of C═C stretching.[27] Therefore, we consider that $\mathbf{b}_2$ and $\mathbf{b}_2'$ belong to a common mode. For the similar reasons, two broad bands $\mathbf{c}_1$ and $\mathbf{c}_2$ of the natural sample are attributed to $\mathbf{c}_1'$ and $\mathbf{c}_2'$ of the ^{13}C-substituted sample [Figs. 5(b) and 5(e), respectively].

The $\mathbf{b}_1$ band is the next lowest-frequency peak in the (a,a)- and (b^*,b^*)-polarized spectra of the natural sample. In the (a,a)-polarized spectrum of the ^{13}C-substituted sample [Fig. 5(a)], no peak corresponds to $\mathbf{b}_1$, but in the (b^*,b^*)-polarized spectrum [Fig. 5(c)] there exists an intense band $\mathbf{b}_1'$. We consider that $\mathbf{b}_1$ and $\mathbf{b}_1'$ belong to a common mode, because these two peaks show an analogous polarization dependence and the frequency difference is in the reasonable range as the isotope shift for the C═C stretching. Since the ^{13}C substitution decreases the stretching frequency of the bare central C═C bond, it will cause a decoupling between the central and ring C═C stretchings, which are coupled in the natural compound. As a consequence, the contribution of the central C═C stretching is enhanced in ν_3 of the substituted sample.[24,25] Since the central C═C bond is oriented along the b^* axis, the Raman intensity of ν_3 for the ^{13}C-substituted sample is expected to be enhanced in the

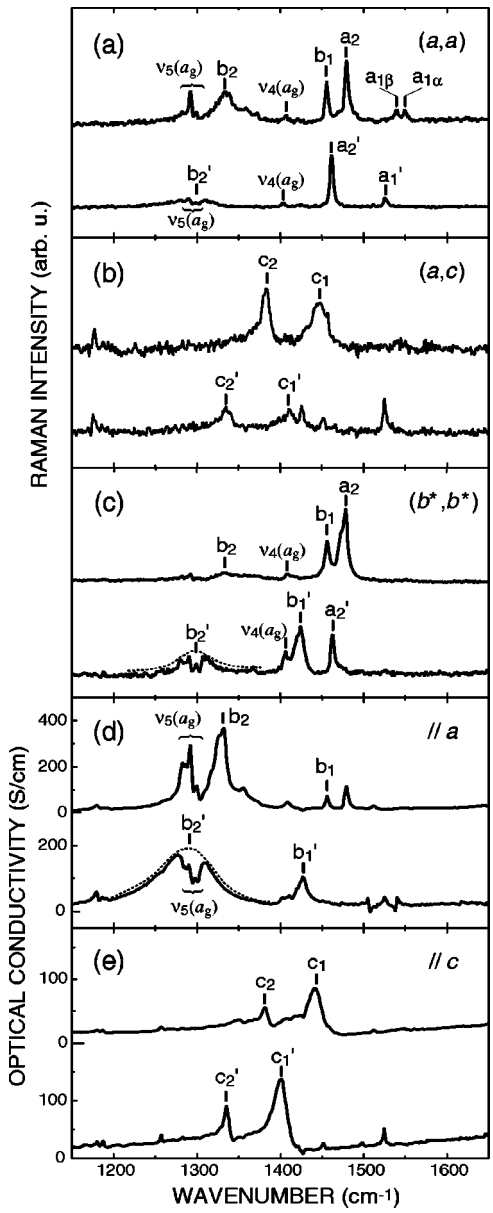

FIG. 5. Polarized Raman and optical-conductivity spectra of the natural (upper curve) and ^{13}C-substituted (lower curve) samples. (a), (b), and (c) show the (a,a)-, (a,c)-, and (b^*,b^*)-polarized Raman spectra, and (d) and (e) show the *a*- and *c*-polarized optical-conductivity spectra, respectively ($T=50$ K). Dashed curves in (c) and (d) are the guide for eyes.

(b^*,b^*) polarization. Accordingly, if we assign $\mathbf{b}_1$ and $\mathbf{b}_1'$ to the ν_3 mode, the different polarization dependence of the two peaks $\mathbf{b}_1$ and $\mathbf{b}_1'$ can be reasonably explained.

The remaining peaks are classified into the high-frequency peaks [$\mathbf{a}_{1x}$ $(x=\alpha,\beta)$ and $\mathbf{a}_1'$] and the low-frequency peaks ($\mathbf{a}_2$ and $\mathbf{a}_2'$). We consider that the peaks classified in the same group belong to the common mode, though the number of peaks in the former group differs between the two samples. We will mention the reason for this disagreement at the end of the following section.

The above classifications are summarized in Table I together with the isotope shifts. As shown in Table I, all peaks can be divided into two groups: the isotope shifts for $\mathbf{a}_1$ and $\mathbf{a}_2$ are smaller than ca. 20 cm^{-1}, whereas those for $\mathbf{b}_1$, $\mathbf{b}_2$, $\mathbf{c}_1$, and $\mathbf{c}_2$ are larger than ca. 30 cm^{-1}. The large difference in the isotope shift clearly indicates that the former peaks are assigned to ν_2 and the latter to ν_3. It should be noted that this assignment agrees with the above tentative assignment for $\mathbf{b}_1$ and $\mathbf{b}_1'$.

TABLE I. Experimental Raman (R) and optical-conductivity (IR) peak-frequencies spectra (cm^{-1}) and the assignments to the C═C stretching modes (Fig. 5). The isotope shift ($\Delta\omega$) is calculated separately for the Raman and IR signals.

Peak	^{12}C		^{13}C		$\Delta\omega$		Assign-
Label	R	IR	R	IR	R	IR	ment
$\mathbf{a}_1$	1548		1525		18[a]		ν_2
	1539						
$\mathbf{a}_2$	1480		1461		19		ν_2
$\mathbf{b}_1$	1455	1456	1424	1427	31	29	ν_3
$\mathbf{c}_1$	1447	1442	1410	1401	37	41	ν_3
$\mathbf{c}_2$	1383	1380	1334	1335	49	45	ν_3
$\mathbf{b}_2$	1333	1328	1290	1291	43	37	ν_3

[a]Calculated using the average frequency of peaks $\mathbf{a}_{1\alpha}$ and $\mathbf{a}_{1\beta}$.

IV. DISCUSSION

A. Factor-group analysis

The vibrational spectrum of crystalline samples often shows more lines than what is expected for the isolated molecule, since the site symmetry is lowered by the low-symmetry environment surrounding the molecules. In the present case, however, such an activation of forbidden modes cannot explain the appearance of the multiple peaks, because the C═C stretching modes consist of only two gerade modes, as has been confirmed in Sec. III A. Therefore, we focus on factor-group splitting to understand the reason for the appearance of the multiple peaks in this section.

As shown in Fig. 1(b), the unit cell of the insulating phase accommodates four molecules. The four molecules are divided into two crystallographically independent pairs, in which A_n and D_n $(n=1,2)$ are crystallographically independent of each other, and X_1 $(X=A,D)$ is connected with X_2 by the screw-axis symmetry, which is parallel to the *a* axis. If the four molecules are nearly equivalent and the intermolecular interaction is negligible, the C═C stretching mode should be fourfold degenerate. On the other hand, if these four molecules are strongly interacting with each other, the molecular vibrations can be coupled to each other to form the combination modes, which results in the unfolding of the degeneracy in accordance with the factor-group symmetry. Table II displays the correlation diagram of the normal modes among the molecular, site, and factor-group symmetry. This table shows that the four modes are split into pairs of the *A* and *B* types of the crystalline modes under the factor-group symmetry C_2 of the insulating phase. Comparison between the experimental results and this table indicates

TABLE II. Correlation diagram of ν_2 and ν_3 among the molecular, site, and factor-group symmetry.

Modes	Mol. sym. D_{2h}	Site sym. C_1	Factor grp. C_2	Corresponding peaks
$4\nu_2$	$4a_g$	$4A$	$2A$	$\mathbf{a}_1, \mathbf{a}_2$
			$2B$	
$4\nu_3$	$4a_g$	$4A$	$2A$	$\mathbf{b}_1, \mathbf{b}_2$
			$2B$	$\mathbf{c}_1, \mathbf{c}_2$
$4\nu_{27}$	$4b_{1u}$	$4A$	$2A$	
			$2B$	

that the polarization dependence of the observed ν_3 signals can be explained by the factor-group symmetry; according to the selection rule for this symmetry, peaks $\mathbf{b}_1$ and $\mathbf{b}_2$ appearing in the (a,a)- and (b^*,b^*)-polarized Raman and a-polarized IR spectra are attributed to the A crystalline mode, and $\mathbf{c}_1$ and $\mathbf{c}_2$ in the (a,c)-polarized Raman and c-polarized IR spectra to the B mode. The clear factor-group splitting observed for ν_3 suggests that this mode induces a strong intermolecular charge oscillation due to the EMV coupling. This argument is consistent with the calculations predicting that ν_3 has the strongest EMV coupling constant among the normal modes of ET^+.[24,28] The broad linewidths of $\mathbf{b}_2$, $\mathbf{c}_1$, and $\mathbf{c}_2$ and strong IR intensity of these peaks also support the present explanation.

On the other hand, clear ν_2 signals were only observed for the A modes. Weaker EMV coupling is responsible for the absence of the B mode, because the coupling constant of this mode is smaller than that of ν_3. The sharp line shapes of $\mathbf{a}_1$ and $\mathbf{a}_2$ also indicate the weak EMV coupling of this mode. The splitting of ν_2 in the A mode is ascribed to CD as we will discuss in the following section. As already mentioned in Sec. III B, the natural sample showed a peculiar doublet, $\mathbf{a}_{1\alpha}$ and $\mathbf{a}_{1\beta}$, in the (a,a)-polarized Raman spectrum [see Fig. 5(a)]. If both $\mathbf{a}_{1\alpha}$ and $\mathbf{a}_{1\beta}$ originate from the ν_2 mode together with $\mathbf{a}_2$, we have to consider a larger unit cell because the factor-group analysis based on the doubled unit cell predicts at most two A modes for one molecular mode. However, a larger unit cell is inconsistent with the reasonable agreement of ν_3 with the factor-group analysis based on the doubled unit cell. Because ν_3, which has a larger EMV coupling constant, should be more sensitive to possible changes in the inter-molecular interaction than ν_2, it seems unreasonable to ascribe the appearance of the doublet to the factor-group splitting. Furthermore, the ^{13}C-substituted sample did not show such an extra ν_2 peak in the A mode [see Fig. 5(b)]. Therefore, we conclude that one of the peaks in the doublet of the natural sample is attributed to an overtone or a combination mode, which is enhanced by the Fermi resonance with the peak corresponding to $\mathbf{a}_1'$ of the ^{13}C-substituted sample.

The fact that the selection rule for the ν_3 signals can be explained by the factor-group analysis based on the symmetry determined by the x-ray diffraction indicates the existence of the screw-axis symmetry in the insulating phase. Since the frequency of the ν_3 mode is sensitive to the charge on the molecule, this result ensures the equivalence of the molecular charge on the crystallographically equivalent molecules. It should be emphasized that the screw-axis symmetry is verified for the charge distribution. Because the spectroscopic method provides higher sensitivity to the molecular charge than the x-ray diffraction method, this result can be a crucial information for the determination of the symmetry of the charge ordering.

B. EMV coupling in the charge-ordered system

The vibronic coupling effect has been analyzed using cluster models which have been applied mainly to 1D systems.[29–31] Since the unit cell of the present 2D system includes four ET molecules [See Fig. 1(b)], we introduce a 2D tetramer to discuss the observed spectral features. The Hamiltonian for the EMV coupling within a tetramer is written as

$$H_{\mathrm{EMV}} = \sum_{i=1,2,3,4} g_i n_i Q_i . \tag{1}$$

In this formula, Q_i denotes the vibrational normal coordinate (in the present discussion, we consider only a_g type modes), n_i indicates the charge population on the ith site among four ETs, and g_i stands for the EMV coupling constant between an unpaired electron at ith site and the vibrational mode. Using the symmetrized normal coordinates $Q_x^{\pm} = (Q_{x1} \pm Q_{x2})/2$ $(X = \mathrm{A,D})$ and the sum or difference of the charge population within the pair $n_x^{\pm} = (n_{x1} \pm n_{x2})/2$, the Hamiltonian is transformed into[31,32]

$$\begin{aligned} H_{\mathrm{EMV}}/g = {} & (Q_{\mathrm{D}}^+ + Q_{\mathrm{A}}^+)(n_{\mathrm{D}}^+ + n_{\mathrm{A}}^+) + (Q_{\mathrm{D}}^+ - Q_{\mathrm{A}}^+)(n_{\mathrm{D}}^+ - n_{\mathrm{A}}^+) \\ & + (Q_{\mathrm{D}}^- + Q_{\mathrm{A}}^-)(n_{\mathrm{D}}^- + n_{\mathrm{A}}^-) + (Q_{\mathrm{D}}^- - Q_{\mathrm{A}}^-)(n_{\mathrm{D}}^- - n_{\mathrm{A}}^-), \end{aligned} \tag{2}$$

where we have neglected the difference in the coupling constant g between the crystallographically independent molecules. Notice that Q^+ and n^+ belong to the A crystalline mode, since Q^+ is the in-phase combination of the normal coordinates, and n^+ is the sum of the charges between the crystallographically equivalent molecules. Thus, the first and second terms of Eq. (2) composed of Q^+ and n^+ belong to the A mode. Similarly, the third and fourth terms belong to the B mode.

Figure 6 shows the schematic level diagram of the EMV coupling in the tetramer. If this compound has a uniform charge distribution (no CD), all ETs should have nearly the same frequency for each normal mode. Therefore, the first term represents the totally in-phase coupled mode, which does not induce charge oscillation between any combination of molecules. Since this mode is decoupled with charge oscillation, its frequency shows no shift [see Fig. 6(b)] from the value determined by the molecular charge. Thus, this Raman-active mode cannot be IR active. The second term represents the in-phase coupling between X_1 and X_2 $(X = \mathrm{A,D})$ and antiphase coupling between A_n and D_n $(n = 1,2)$. In contrast to the first term, the second term induces the charge oscillation between A_n and D_n, and thus this

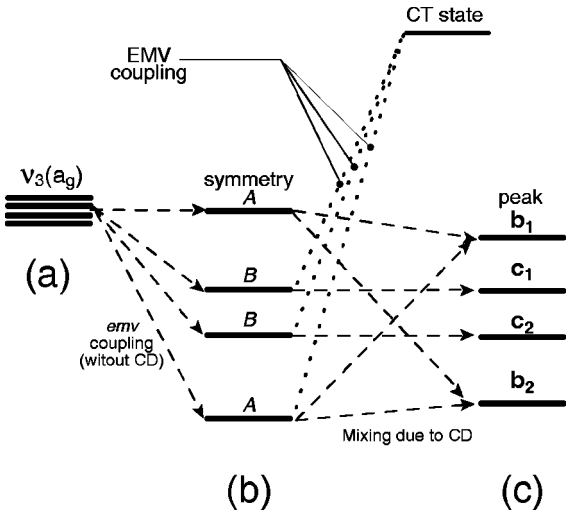

FIG. 6. Level diagram of the EMV coupling effects. (a) Molecular normal modes are degenerated in isolated states. (b) The degenerated modes are split into one EMV-uncoupled and three EMV-coupled modes in the presence of the vibronic interaction. The dotted lines indicate the interaction with the CT state caused by the second to fourth terms in Eq. (2). (c) The charge disproportionation mixes the two *A*-symmetry modes and turns the originally in-phase mode to be IR active.

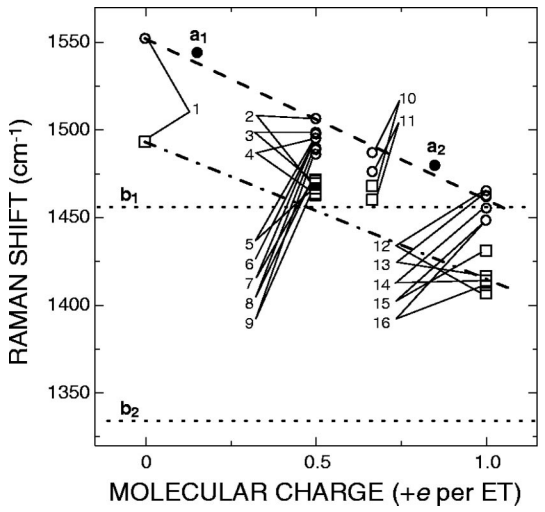

FIG. 7. Reported Raman frequencies of ν_2 (circles) and ν_3 (squares) for various ET salts listed in Table III. The data are plotted with respect to the ET molecular charge. Broken and dotted-broken lines show the approximate charge dependence of the two modes. The two dotted lines show the frequencies of $\mathbf{b}_1$ and $\mathbf{b}_2$ (see text).

Raman-active mode can be IR active. This vibronic level will show a down-shift as shown in Fig. 6(b). Consequently, if CD is not present, one IR and two Raman bands will be observed as the *A* mode [$E\|a$ for IR and (a,a) and (b^*,b^*) for Raman]. On the other hand, if CD is present, the frequency of the charge-sensitive C═C stretching mode should be different between the A_n and D_n sites. This difference leads to a mixing of the states coming from the first and the second terms in Eq. (2) [see Fig. 6(c)], and thus the originally IR inactive mode based on the first term gains the IR intensity from that of the second term. Recall that there exist two *A* modes of ν_3 ($\mathbf{b}_1$ and $\mathbf{b}_2$) in the observed IR spectra [Fig. 5(d)]. The weaker intensity of $\mathbf{b}_1$ suggests that this peak corresponds to the IR-activated mode. Appearance of this mode in the IR spectrum can be viewed as a proof for the occurrence of CD in this insulating phase. In Sec. IV A, we verified that this crystal has a screw-axis symmetry in the charge distribution. Thus, we conclude that the separated charge forms a so-called horizontal pattern running along the screw axis ($\|a$ axis).

C. Charge disproportionation ratio

Many charge-sensitive modes linearly change the frequency, depending upon the charge on the molecule. Utilizing this property, the fractional molecular charge in CT salts is often estimated from the frequency shift of such modes.[15–18] For the ET molecule, it is known that the two gerade C═C stretchings ν_2 and ν_3 show a large charge-dependent frequency shift. However, as we have discussed so far, the two modes show the different vibronic properties. In order to estimate the molecular charge from the vibrational frequency, we have to take into account the EMV coupling effect.

The effect of the EMV interaction appears strongly in the spectrum only when the intermolecular CT interaction and the coupling constant of the specific vibration mode are strong enough. Therefore, we can classify the signals from the charge-sensitive modes in terms of the properties related to the molecular vibrational modes and the crystalline electronic state to understand the influence of the EMV coupling. The molecular vibrational mode is characterized by the charge sensitivity of the frequency and strength of the coupling constant of EMV interaction. Because the charge-insensitive mode is useless here, we discuss the charge-sensitive modes with (a) weak and (b) strong coupling constant. The crystalline electronic state is characterized by the charge distribution and the strength of the inter-molecular CT interaction, and classified into four cases: (i) uniform distribution and weak CT interaction, (ii) CD and weak CT interaction, (iii) uniform distribution and strong CT interaction, and (iv) CD and strong CT interaction. In the case of (i) and (ii), the molecular charge can be estimated without any consideration on the EMV coupling; we can use both (a) and (b) types of vibrational modes for this purpose. On the other hand, in the case of (iii) and (iv), we have to take account of the frequency shift due to the EMV interaction. For the (iii) case, the totally in-phase modes uncoupled with the vibronic effects. Thus, both (a)- and (b)-type modes are available as a reliable measure of the molecular charge [see Fig. 6(b)]. In the case of (iv), however, because the in-phase mode is also involved in the EMV interaction, we can use only the (a)-type modes. Since the insulating phase of the present compound belongs to (iv), it is suspected that ν_3 showing the strong EMV coupling effect is inappropriate for the estimation of the molecular charge (CD ratio). Meanwhile, we have confirmed that the ν_2 shows weaker EMV coupling features. It suggests that this mode can be applied to the CD ratio estimation as a (a)-type mode.

Figure 7 displays the Raman frequencies of ν_2 and ν_3

TABLE III. Raman frequencies (cm^{-1}) of ν_2 and ν_3 plotted in Fig. 7. For those peaks which appear as split peaks or have a shoulder, the higher frequency is adopted as the peak position (refer to the original papers), because the peak of the lower frequency may be influenced by the EMV coupling.

Number	Compound	ρ (e)	ν_2	ν_3	Ref.
1	Neutral ET	0	1552	1494	33
2	κ-$(ET)_2[Cu(NCS)_2]$	0.5	1506	1470	34
3	κ-$(ET)_2Cu_2(CN)_3$	0.5	1498	1471	16
4	κ-$(ET)_2Cu[N(CN)_2]Br$	0.5	1496	1468	25
5	β-$(ET)_2I_3$	0.5	1495	1468	35
6	κ-$(ET)_2Cu[N(CN)_2]Cl$	0.5	1489	1463	16
7	α-$(ET)_2(NH_4)Hg(SCN)_4$	0.5	1488	1469	16
8	α-$(ET)_2RbHg(SCN)_4$	0.5	1488	1469	16
9	κ-$(ET)_4Hg_3Cl_8$	0.5	1486	1464	16
10	$(ET)_3Cl_2 \cdot H_2O$	0.67	1487	1468	16
11	$(ET)_3(HSO_4)_2$	0.67	1476	1460	16
12	$(ET)BiI_4$	1	1465	1407	16
13	$(ET)AuBr_2Cl_2$	1	1462	1416	16
14	$(ET)_2[Mo_6O_{19}]$	1	1460	1414	36
$\mathbf{a}_1$	θ-$(ET)_2RbZn(SCN)_4$	0.15	1544		Present study
$\mathbf{b}_2$	θ-$(ET)_2RbZn(SCN)_4$	0.85	1480		Present study

(see also Table III) for various ET based CT salts plotted against the molecular charge expected from the stoichiometry.[16,25,33–36] The broken ν_2 and dot-broken ν_3 lines were drawn between the frequencies of the neutral molecule and monocations. This figure manifests that the frequencies of ν_3 signals show an irregular molecular-charge dependence, i.e., peak $\mathbf{b}_2$, for instance, is positioned much lower than that of ν_3 for the monocationic ET. On the other hand, the frequencies of the two A modes of ν_2 are included within those of the neutral and monocationic ETs, suggesting that this mode can be applicable to the CD ratio estimation. Using the slope 90 cm^{-1}/e of the broken line, we estimated the deviation ρ from the average charge $(+0.5e)$ of the two types of molecules $A^{+(0.5-\rho)}$ and $D^{+(0.5+\rho)}$ as $\rho \approx +0.35$ (black circles in Fig. 7). The CD ratio determined from the above analysis is thus $+0.15e:+0.85e$. This ratio is almost the same to the value estimated by the NMR experiment.[7] Agreement of the two individual measurements strongly support the reliability of the estimated value and the plausibility of the molecular-charge-estimation method based on ν_2.

V. CONCLUSION

We measured the IR and Raman spectra of θ-$(ET)_2RbZn(SCN)_4$ in the insulating phase, and investigated the charge distribution through the interpretation of the multiple C=C stretching bands. We assigned four ν_3 crystal modes and two ν_2 crystal modes based on the spectra of the ^{13}C-substituted compound and factor-group analysis. The ν_3 mode, which is strongly coupled with electronic systems, was employed to verify the occurrence of CD and the symmetry of the charge distribution. On the other hand, the ν_2 mode, which is weakly coupled, was used for the CD ratio estimation. The present result is important not only to confirm the occurrence of the charge ordering in the insulating phase of this compound, but also to understand the vibrational spectra in charge-ordered systems with strong EMV interaction.

ACKNOWLEDGMENTS

We wish to thank to Dr. O. Drozdova, Dr. M. Maksimuk, and Dr. R. Wojciechowski of Institute for Molecular Science and Dr. M. Inokuchi of Science University of Tokyo in Yamaguchi for their helpful discussion. This study was supported by the Ministry of Education, Science, Sports and Culture of Japan: a Grant-in-Aid for the Encouragement of Young Scientists (No. 12740392) and a Grant-in-Aid for Scientific Research on Priority Areas (B) of Molecular Conductors and Magnets (Area No. 730/No. 11224212).

*Electronic address: yamamoto@ims.ac.jp

[1] K. Hiraki and K. Kanoda, Phys. Rev. Lett. **80**, 4737 (1998).
[2] D. S. Chow, F. Zamborszky, B. Alavi, D. J. Tantillo, A. Baur, C. A. Merlic, and S. E. Brown, Phys. Rev. Lett. **85**, 1698 (2000).
[3] H. Mori, S. Tanaka, and T. Mori, Phys. Rev. B **57**, 12 023 (1998).
[4] H. Mori, S. Tanaka, T. Mori, A. Kobayashi, and H. Kobayashi, Bull. Chem. Soc. Jpn. **71**, 797 (1998).
[5] K. Kanoda, Hyperfine Interact. **104**, 235 (1997).
[6] T. Nakamura, W. Minagawa, R. Kinami, and T. Takahashi, J. Phys. Soc. Jpn. **69**, 504 (2000).
[7] K. Miyagawa, A. Kawamoto, and K. Kanoda, Phys. Rev. B **62**, R7679 (2000).
[8] R. Chiba, H. M. Yamamoto, K. Miraki, T. Nakamura, and T. Takahashi, Synth. Met. **120**, 919 (2001).
[9] H. Seo and H. Fukuyama, J. Phys. Soc. Jpn. **67**, 1848 (1998).
[10] H. Seo, J. Phys. Soc. Jpn. **69**, 805 (2000).

[11] T. Mori, Bull. Chem. Soc. Jpn. **73**, 2243 (2000).
[12] P. Guionneau, C. J. Kepert, G. Bravic, D. Chasseau, M. R. Truter, M. Kurmoo, and P. Day, Synth. Met. **86**, 1973 (1997).
[13] T. Hatsui, K. Okamoto, T. Yokoyama, Y. Kitajima, H. Tanaka, E. Ojima, A. Kobayashi, and T. Ohta, Chem. Phys. Lett. **330**, 309 (2000).
[14] J. Ouyang, K. Yakushi, Y. Misaki, and K. Tanaka, Phys. Rev. B **63**, 054301 (2001).
[15] O. Drozdova, H. Yamochi, K. Yakushi, M. Uruichi, S. Horiuchi, and G. Saito, J. Am. Chem. Soc. **122**, 4436 (2000).
[16] H. H. Wang, R. Ferraro, J. M. Williams, U. Geiser, and A. Schlueter, J. Chem. Soc. Chem. Commun. , 1893 (1994).
[17] H. H. Wang, A. M. Kini, and J. M. Williams, Mol. Cryst. Liq. Cryst. Sci. Technol., Sect. A **284**, 211 (1996).
[18] J. Moldenhauer, Ch. Horn, K. I. Pokhodnia, D. Schweitzer, I. Heinen, and H. J. Keller, Synth. Met. **60**, 31 (1993).
[19] T. Nakamura, W. Minagawa, R. Kinami, Y. Konishi, and T. Takahashi, Synth. Met. **103**, 1898 (1999).
[20] K. Yakushi, Bull. Chem. Soc. Jpn. **73**, 2643 (2000).
[21] J. E. Eldridge, Y. Xie, J. A. Schlueter, J. M. Williams, D. Naumann, and T. Roy, Solid State Commun. **99**, 335 (1996).
[22] In the space group $I222$, the vibronic band is IR forbidden.
[23] H. Tajima, S. Kyoden, H. Mori, and S. Tanaka, Phys. Rev. B **62**, 9378 (2000).
[24] M. E. Kozlov, K. I. Pokhodnia, and A. A. Yurchenko, Spectrochim. Acta, Part A **45**, 437 (1989).
[25] J. E. Eldridge, C. C. Homes, J. M. Williams, A. M. Kini, and H. H. Wang, Spectrochim. Acta, Part A **51**, 947 (1995).
[26] J. E. Eldridge, Y. Xie, H. H. Wang, J. M. Williams, A. M. Kini, and J. A. Schlueter, Mol. Cryst. Liq. Cryst. Sci. Technol., Sect. A **284**, 97 (1996).
[27] The upper limit ($60\ \mathrm{cm}^{-1}$) is determined by the isotope shift of an imaginary isolated C═C bond given by $(\sqrt{13/12}-1)\times\omega_{\mathrm{C=C}}$, where $\omega_{\mathrm{C=C}}$ is supposed to be ca. $1500\ \mathrm{cm}^{-1}$.
[28] K. I. Pokhodnia, M. E. Kozlov, V. G. Onischenko, D. Schweitzer, J. Moldenhauer, and R. Zamboni, Synth. Met. **55-57**, 2364 (1993).
[29] V. M. Yartsev and R. Swietlik, Rev. Solid State Sci. **4**, 69 (1990).
[30] R. Bozio, A. Feis, D. Pedron, I. Zanon, and C. Pecile, in Lower-Dimensional Systems and Molecular Electronics, edited by R. M. Metzger *et al.* (Plenum, New York, 1991), 23.
[31] M. Meneghetti and C. Pecile, Phys. Rev. B **40**, 12 187 (1989).
[32] A. Girlando, R. Bozio, C. Pecile, and J. B. Torrance, Phys. Rev. B **26**, 2306 (1982).
[33] M. E. Kozlov, K. I. Pokhodnia, and A. A. Yurchenko, Spectrochim. Acta, Part A **43**, 323 (1986).
[34] R. Swietlik, C. Garrigou-Lagrange, C. Sourisseau, G. Pages, and P. Delhaes, J. Mater. Chem. **2**, 857 (1992).
[35] S. Sugai and G. Saito, Solid State Commun. **58**, 759 (1986).
[36] G. Visentini, M. Masino, C. Bellitto, and A. Girlando, Phys. Rev. B **58**, 9460 (1998).